From crystal to glass-like thermal conductivity in crystalline minerals

Yohan Bouyrie, Christophe Candolfi, Stéphane Pailhes, Michael Marek Koza, Bernard Malaman, Anne Dauscher, Janusz Tobola, Olivier Boisron, Lucien Saviot, Bertrand Lenoir

From Crystal to Glasslike Thermal Conductivity in Crystalline Minerals

Y. Bouyrie[1], C. Candolfi[1,*], S. Pailhès[2], M. M. Koza[3], B. Malaman[1], A. Dauscher[1], J. Tobola[4], O. Boisron[2], L. Saviot[5], B. Lenoir[1]

[1] *Institut Jean Lamour, UMR 7198 CNRS – Université de Lorraine, Parc de Saurupt, CS 50840, 54011 Nancy, France*

[2] *Institute of Light and Matter, UMR 5306 Université Lyon 1-CNRS, Université de Lyon 69622 Villeurbanne cedex, France*

[3] *Institut Laue Langevin, 6 rue Jules Horowitz, B.P. 156, 38042 Grenoble, Cedex 9, France*

[4] *Faculty of Physics and Applied Computer Science, AGH University of Science and Technology, 30–059 Krakow, Poland*

[5] *Laboratoire Interdisciplinaire Carnot de Bourgogne (ICB), UMR 6303 CNRS-Université de Bourgogne Franche-Comté, 9 avenue A. Savary, BP 47870, F-21078, Dijon Cedex, France*

[*]Corresponding authors: christophe.candolfi@univ-lorraine.fr

PACS numbers: 63.20.Ry, 78.70.Nx, 91.60.Ki

Abstract

The ability of some materials with perfectly ordered crystal structure to mimic the heat conduction of amorphous solids is a remarkable physical property that finds applications in numerous areas in material's science such as in the search of more efficient thermoelectric materials that enable to directly convert heat into electricity. Here, we unveil the mechanism from which, glass-like thermal conductivity emerges in tetrahedrites, a family of natural minerals extensively studied in geology and, more recently, in thermoelectricity. By investigating the lattice dynamics of two tetrahedrites of very close compositions ($Cu_{12}Sb_2Te_2S_{13}$ and $Cu_{10}Te_4S_{13}$) but with opposite glasslike and crystal thermal transport by means of powder and single-crystal inelastic neutron scattering, we demonstrate that the former originates from the peculiar chemical environment of the copper atoms giving rise to strongly anharmonic excess of vibrational states.

I. Introduction

The search for materials that enable to either optimize heat transfer or minimize waste heat is crucial in all thermal energy conversion processes. New crystalline materials with a very low ability to transport heat have a direct impact on the energy conservation. They are employed as thermal barriers and operate in optical phase-change memories or in thermoelectric devices.[1-5] In this last area of research, semiconducting materials with a low lattice thermal conductivity, k_L, are intensively sought.[3,4] Minimizing k_L, however, rests on identifying microscopic mechanisms that enable to dissipate the energy of heat-propagating phonons thereby disrupting efficiently the heat transport.

Besides amorphous systems that are natural thermal insulators due to their inherent structural disorder, numerous crystalline compounds exhibit anomalously low k_L.[6-10] The microscopic mechanisms from which, this surprising behaviour emerges have been the subject of a large body of theoretical work, accompanied by extensive experimental studies. These investigations have led to a rich diversity in physical scenarios. Among others, guest-host interaction in cage-like materials, the nearness of a ferroelectric-like lattice instability in PbTe, or nanostructure (spontaneous or artificial) in $AgSbTe_2$ are all prominent examples of mechanisms that significantly reduce k_L.[11-20] As recently reviewed by Nielsen *et al.*[16], s^2 lone-pair electrons on the groups V and VI metalloid atoms represent another extremely efficient scattering channel of heat-carrying phonons that strongly lower k_L in crystalline solids over a wide temperature range. In some specific cases, the lone *s*-electrons revolving around these atoms can be stereo-chemically active *i.e.* they participate in the bonding with the neighbouring atoms forming polar covalent bonds, thereby influencing the eigenwaves of atomic motion, known as phonons, in the crystal. The presence of lone pairs is believed to

substantially enhance the phonon anharmonicity known to be the main source of resistance to heat conduction.[9,21-23] This mechanism is believed to be at the origin of the anomalously low lattice thermal conductivity observed in tetrahedrites. However, the underlying microscopic mechanisms responsible for the glass-like thermal transport in these minerals lack direct experimental evidence.

In this paper, we provide this key experimental observation by measuring and comparing the vibrational properties of two tetrahedrites of very close composition, namely $Cu_{12}Sb_2Te_2S_{13}$ and $Cu_{10}Te_4S_{13}$, by means of temperature-dependent inelastic neutron scattering (INS) and Raman spectroscopy. The glass-like thermal transport observed in $Cu_{12}Sb_2Te_2S_{13}$ evolves towards a conventional, crystal-like behaviour in $Cu_{10}Te_4S_{13}$. It is this trait that marks these two isotructural tetrahedrites as distinct and points to fundamental differences in their phonon scattering processes. Our results provide conclusive experimental evidences of an additional very low-energy vibrational mode in $Cu_{12}Sb_2Te_2S_{13}$ with respect to $Cu_{10}Te_4S_{13}$ that we assign to the vibrations of copper atoms surrounded by two Sb/Te atoms. Our results show that the unusual three-fold coordination environment of the Cu2 atoms plays an important role in lowering k_L in $Cu_{12}Sb_2Te_2S_{13}$. Intriguingly, this mode exhibits a strong renormalization of its characteristic energy towards higher energies upon heating from 2 K to 500 K, a behaviour commonly considered a hallmark of rattling anharmonicity. The extremely low energy of these vibrations, coupled with the heat-carrying phonons, is a remarkable dynamical property responsible for the drastic reduction of the phase space available for acoustic phonon states and for phonon-phonon scattering processes. In turn, the lack of such feature in the ternary $Cu_{10}Te_4S_{13}$ provides a simple explanation of the conventional behaviour of k_L. The microscopic picture unveiled herein is a general mechanism from which, extremely low, glass-like thermal conductivity can emerge in natural and synthetic tetrahedrites.

II. Experimental details

A. Sample preparation and characterization

Polycrystalline samples of $Cu_{12}Sb_2Te_2S_{13}$ and $Cu_{10}Te_4S_{13}$ were prepared by powder metallurgy using elemental Cu powders (99.999%, ChemPur), S powders (99.999%, StremChemicals), Sb shots (99.999%, 5NPlus) and Te shots (99.999%, 5NPlus) as starting materials. All manipulations of elements were conducted in a dry, argon-filled glove box. The elements were loaded in stoichiometric amounts in evacuated quartz ampules, sealed under secondary vacuum and placed in a vertical furnace. The ampules were heated up to 650°C at a rate of 0.3°C.min^{-1} due to the low vapour pressure of sulphur. The tubes were dwelt at this temperature for 24h and cooled down to room temperature at a rate of 0.4°C.min^{-1}. The obtained ingots were grounded into fine powders, cold-pressed into cylindrical pellets and further annealed at 450°C for one week. The final product was eventually crushed into micron-sized powders.

Powder X-ray diffraction (PXRD) was carried out with a Bruker D8 Advance diffractometer using CuKα1 radiation (/ = 1.54056 Å). Rietveld refinements on the measured patterns were performed using the Fullprof software (see Electronic Supplementary Information, Figure 1). The structure determination of both tetrahedrites was performed at 300 K on single-crystals easily extracted from the as-cast ingots. Diffraction data were collected on a Kappa APEX II diffractometer using MoKα radiation (/ = 0.71073 Å) and CCD area detector. The structural refinements were carried out using the SHELX97 software. The atomic positions and thermal displacement parameters of each atom are summarized in Tables 1 and 2 (see Electronic Supplementary Information) for $Cu_{10}Te_4S_{13}$ and $Cu_{12}Sb_2Te_2S_{13}$, respectively, while the relevant interatomic distances and bond angles are listed in Table 3. Of note, in the two compounds, no superstructure was observed indicating that both Te atoms in $Cu_{12}Sb_2Te_2S_{13}$ and vacancies in $Cu_{10}Te_4S_{13}$ are randomly distributed within the crystal

structure, in agreement with prior studies. Furthermore, in $Cu_{10}Te_4S_{13}$, the vacancies mainly occupy the Cu2 sites (Tables 1 and 2). The presence of a slight fraction of elemental Te in this sample might hint at possible slight off-stoichiometry on the Te and/or Cu site.

B. Thermal conductivity measurements

Thermal conductivity measurements were performed on bulk dense samples consolidated by spark plasma sintering (SPS) at 450°C under 80 MPa for 10 minutes. The experimental density of both samples was measured to be above 95% of the theoretical density. PXRD patterns collected after the densification process were found to be similar to those of the premade powders evidencing the absence of thermal decomposition during the SPS treatment. The thermal conductivity was measured using the thermal transport option of the PPMS between 5 and 300 K. The contacts were realized by attaching four coppers leads onto the samples using thermally conducting silver epoxy. To ensure mechanically-stable contacts, the (samples + copper leads) were maintained for 20 minutes at 130°C. The data were corrected for thermal radiations by a model implemented in the TTO option software by Quantum Design. Despite this correction, above 250 K, thermal radiations give a slight contribution to the measured values. This is seen in the high-temperature data measured on both compounds by a laser flash technique to determine the thermal diffusivity (LFA 427, Netzsch). The thermal conductivity is then obtained by multiplying the thermal diffusivity, the experimental density and the specific heat (measured in the same temperature range by differential scanning calorimetry using a DSC 403 F3 from Netzsch). At 300 K, these measurements yielded $\kappa \approx$ 0.55 and 1.0 $W.m^{-1}.K^{-1}$ for $Cu_{12}Sb_2Te_2S_{13}$ and $Cu_{10}Te_4S_{13}$, respectively.

C. Inelastic neutron scattering and Raman scattering

Inelastic neutron scattering measurements were performed on powdered samples with the time-of-flight spectrometers IN4@ILL and IN6@ILL at the European neutron source Institut Laue Langevin (ILL) in Grenoble, France. IN6@ILL was utilized with an incident neutron wavelength of 4.14 Å in the time focusing mode with the best energy resolution sets to 7.5 meV at the anti-Stokes line. The inelastic response of $Cu_{12}Sb_2Te_2S_{13}$ was recorded at 50, 100, 200, 300 and 500 K. Measurements at 2, 50, 100 and 200 K were carried out on both compounds at IN4@ILL with an incident neutron wavelength of 2.2 Å at the Stokes line. Standard correction procedures were applied to the data. They comprised empty sample holder and background corrections, normalization to vanadium standard for detector efficiency corrections and a rescaling for energy-dependent count efficiencies. The corrected data were converted to the scattering function $S(Q,\omega)$, which was further processed to derive the generalized density of states $G(\omega)$. All the calculations were performed within the incoherent approximation. The peak positions of the phonon modes observed in $G(\omega)$ were approximated by Gaussian least-square fits.

The Stokes and anti-Stokes Raman spectra were simultaneously recorded down to 12 cm^{-1} with an excitation of 532 nm using a Renishaw inVia setup together with a BragGrate notch filter from OptiGrate.

D. Neutron 3-axis scattering

Wavelengths and energies of both acoustic and optical phonons were probed in a natural, single-crystalline tetrahedrite specimen ($Cu_{10}Fe_{0.4}Zn_{1.6}As_{3.7}Sb_{0.3}S_{13}$) by means of triple axis neutron spectroscopy. The measurements were taken at the thermal 2T triple axis spectrometer at the Laboratoire Léon Brillouin (Saclay, France). A focusing pyrolytic graphite

(PG) (002) monochromator and analyser were used. A PG filter was inserted into the beam in order to eliminate higher order contamination. The crystal was oriented such that momentum transfers Q of the form $Q = (h, h, l)$ were accessible. We use a notation in which Q is indexed in units of the conventional reciprocal lattice of the body centred cubic structure with $4\pi/a = 1.21$ Å^{-1}. As these measurements were performed on a natural specimen, a rather large momentum resolution $\Delta Q^{FWHM} \sim 0.15$ Å^{-1} was observed due to variations in the chemical composition which lead to a distribution of lattice parameters in the crystal. The resulting Bragg mosaicity measured on the Bragg peak (044) was about ~1.5°. Hence, these measurements allow for observing the phonon dispersions but do not enable analysing in detail the phonon profiles.

III. Results

A. X-ray diffraction and thermal conductivity

Tetrahedrites are natural minerals found as a minor ore of Cu at several places all over the world.[24] Discovered in the 19th century and extensively studied by mineralogists over the last 60 years, it is not until recently, however, that their thermoelectric properties were examined in detail.[25-29] Tetrahedrites crystallize in a cubic crystal structure (space group $I\bar{4}3m$) with 58 atoms per unit cell distributed over five independent crystallographic sites (Fig. 1a, inset). Cu atoms are located in two distinct sites: six Cu1 are tetrahedrally coordinated by sulphur S1 and six Cu2 are in a planar triangle arrangement to two S1 and one S2 atoms. The sulphur atoms S1 are octahedrally coordinated by Cu2 and located at the « corners » of the cubic structure, while the sulphur S2 atoms are in tetrahedral sites bonded to one of the Cu2 atoms in 3-fold coordination, two Cu1 atoms in 4-fold coordination and one Sb atom. Finally, the Sb atoms also occupy tetrahedral sites and are coordinated to three sulphur S1.

First reports demonstrated that tetrahedrites inherently show extremely low, glass-like thermal conductivity values, should they be synthetic or natural.[25-29] As shown in Fig. 1b, $Cu_{12}Sb_2Te_2S_{13}$ does not represent an exception to this behaviour as indicated by the smooth increase in k_L with temperature and the extremely low values measured, of the order of 0.7 $W.m^{-1}.K^{-1}$ at 300 K. This dependence strikingly contrasts with that of $Cu_{10}Te_4S_{13}$, which features a two-fold increase in k_L values and a well-defined low-temperature crystalline peak. Of note, because both compounds are semiconducting with high electrical resistivities at 300 K, the k values solely reflect the lattice contribution k_L.

In order to understand the basic features at the origin of this difference, we first focus on the structural differences between these two tetrahedrites. Single crystal X-ray diffraction measurements performed at room temperature reveal striking differences in the atomic displacement parameters (ADP) of one of the two types of copper atoms contained in the crystal structure and usually referred to as Cu2 (see Tables 1 and 2 in Supplemental Material). The neighbouring atomic environment of the Cu2 atoms, drawn in an ellipsoid representation to highlight the ADPs, are illustrated in Figure 1b for both materials. The perspective view is scaled according to our structural refinements (see Figure 1 in Electronic Supplementary Information). The Cu2 atoms are threefold coordinated to sulphur in a planar triangle. Their ADPs are anisotropic with the largest amplitude along the out-of-plane direction where two apical metalloids atoms (Sb and Te) are located. The atomic displacement parameter of Cu2 in this direction is found to be almost three times larger in $Cu_{12}Sb_2Te_2S_{13}$ than in $Cu_{10}Te_4S_{13}$. This difference can be first regarded as a direct consequence of the decrease in the unit cell volume in the latter owing to the presence of two vacancies per formula unit, which implies a concomitant contraction of the planar triangle and expansion of the distance between Cu2 and the apical metalloids.

B. Lattice dynamics

The strongest experimental evidence of significant differences in the microscopic mechanisms governing the thermal transport is provided by a comparison of the generalized vibrational density of states (GVDOS, $G(\omega)$) measured by inelastic neutron scattering at room temperature in both tetrahedrites (Fig. 2a). The GVDOS represents the sum of all phonon eigenstates of equal energy accessed in the scattering experiment. The main difference between the two inelastic responses clearly emerges at low energies ($\hbar\omega \leq 6$ meV) where an exalted excess of vibrational modes located at about 3 meV is exclusively present in $Cu_{12}Sb_2Te_2S_{13}$. This finding is consistent with the analysis of the specific heat of the $Cu_{10}Zn_2Sb_4S_{13}$ tetrahedrite realized by Lara-Curzio *et al.*[30] and with the vibrational density of states calculated by Lai *et al.*[31] in the $Cu_{12}Sb_4S_{13}$ tetrahedrite revealing quasilocalized modes predominately associated to Cu2 atoms at around 4 meV. Additional experimental evidence of this excess is presented in Fig. 2b, in which the results of Raman scattering are shown. This spectroscopic tool allows for selectively probing the optical vibrations at the centre of the Brillouin zone (Γ point). A clear excess of vibrational modes is observed in $Cu_{12}Sb_2Te_2S_{13}$ in the low-energy region ($\hbar\omega \leq 6$ meV) with respect to $Cu_{10}Te_4S_{13}$. This observation strongly indicates that this excess can be ascribed to the out-of-plane and non-polar optical vibrations of the Cu2 atoms as predicted theoretically by Lu *et al.*[25]. This assignment is further corroborated by the temperature dependence of the ADPs of Cu2 atoms in $Cu_{12-x}Ni_xSb_4S_{13}$ tetrahedrites reported by Suekuni *et al.*[28] which showed the largest values *i.e.* the characteristic energies of their thermal vibrations are the lowest and should thus give rise to features in the GVDOS spectrum at the lowest energies.

The interaction between these optical vibrations and the heat-carrying acoustic waves was investigated by mapping the energy – wavelength phase space of both optical and acoustic phonons in a natural, single-crystalline tetrahedrite specimen. The chemical

composition of the mineral slightly differs from the present synthetic samples but displays similar glass-like thermal properties allowing for a reasonable comparison of experimental data. The dispersions of transverse acoustic phonons (TA) propagating along the high symmetry Γ – H (100) direction, and polarized in the (011) direction, were investigated by performing energy scans around the Bragg peak (044). Constant energy scans were collected between 0 and 17 meV for a set of regularly spaced wave vectors (every 0.12 $Å^{-1}$) covering two entire Brillouin zones. The data are represented as a false colour image in Fig. 3a with subtracted background (see also Figure 2 in Electronic Supplementary Information). A scan of the raw data as a function of the energy is shown in Fig. 3b at the wave vectors q_1 corresponding to a cut through the dispersion curves as depicted by the vertical white lines in Fig. 3a. These measurements demonstrate the existence of a strong scattering process between the dispersive TA phonons and a non-dispersive mode described by a Gaussian centred at 3.5 meV with an intrinsic FWHM of 2.4 meV. The latter mode has been ascribed to the optical out-of-plane vibrations of the Cu2 atoms. The intensity of the acoustic phonons is nearly fully suppressed and their dispersion is interrupted in the energy interval [3.5 – 6 meV]. Above 6 meV, acoustic phonon peaks are retrieved with a strong broadening of their energy widths (*i.e.* life times) along with a deviation of their energy positions from the linear dispersion. Below 3.5 meV, a strong bending of the linear acoustic dispersion is found when approaching the energy of the optical phonon at 3.5 meV. The slope of the TA linear dispersion (*i.e.* the transverse sound velocity) is roughly estimated to be about 1450 $m.s^{-1}$. This value is consistent with that inferred from the measurements of the elastic moduli by ultrasound resonant spectroscopy on a synthetic $Cu_{12}Sb_4S_{13}$ specimen (1577 $m.s^{-1}$).[32] These results clearly show that acoustic phonons strongly couple with a non-dispersive optical branch located at 3 meV in agreement with the energy of the out-of-plane optical vibrations of the Cu2 atoms measured in $Cu_{12}Sb_2Te_2S_{13}$.

As demonstrated recently in the Si-based clathrate Ba_8Si_{46} (Ref. 13), such optical phonons, arising from collective oscillations of atoms with large atomic displacements, substantially impact the propagation of acoustic phonons. This leads to a drastic suppression of the phase space available for heat-carrying phonon states of energies higher than the energy of the lowest optical phonons, thereby strongly lowering the lattice thermal conductivity. Similarly, the difference between the lattice thermal conductivities of both tetrahedrites, as evidenced in Fig. 1a, is a consequence of such effect induced by the additional optical vibrational states observed in $Cu_{12}Sb_2Te_2S_{13}$ and associated with the out-of-plane motion of the Cu2 atoms.

The limit of the acoustic regime is found at a phonon wave vector (q_c) at which, a crossing of the linear acoustic dispersion and the non-dispersive Cu2 optical phonon branch occurs. q_c is estimated by $q_c = E_c / v_{ac}$ where E_c is the energy of the lowest optical phonon and v_{ac} is the sound velocity of the acoustic phonons (transverse or longitudinal).[13] From the energy of the excess mode in the GVDOS and from the sound velocity of the transverse acoustic branch measured in the single-crystalline tetrahedrite, the limit of the acoustic regime in $Cu_{12}Sb_2Te_2S_{13}$ is estimated to $q_c \sim 0.35$ Å^{-1}. This results in a critical reduction of the phase space available for phonon-phonon scattering processes, whose disappearance upon cooling gives rise to the well-known "crystalline peak" in k_L (see Fig. 1a). The above-mentioned value of q_c is very close to $\frac{G}{4} = \frac{1}{4}\left(\frac{4\pi}{a}\right) = \frac{1}{4}\left(\frac{4\pi}{10.3502}\right) \approx 0.30$ Å^{-1} (G is a reciprocal lattice vector of the conventional *bcc* unit cell of lattice parameter a) that corresponds to the minimum value of the phonon wave vectors required to satisfy the condition of the momentum conservation for a three-phonon Umklapp scattering event.[21] Although these usual Umklapp processes are frozen, the presence of a low-energy dispersionless optical branch of phonons in $Cu_{12}Sb_2Te_2S_{13}$ opens an additional channel of Umklapp scattering processes. This

new channel has been first discussed by Lee *et al.*[33] and recently confirmed by *ab initio* calculations (Ref. 34) and can be formulated as "acoustic + optical ⇔ optical phonons". These Umklapp scattering processes are thus more easily achieved at low temperatures giving rise to the amorphous-like dependence of the lattice thermal conductivity.

To determine the degree of anharmonicity of the Cu2 out-of-plane vibrations and its impact on the thermal conductivity, the evolution of the inelastic response as a function of temperature has been followed from 500 K down to 2 K. The GVDOS of both tetrahedrites are depicted in Figs. 4a and 4b. In $Cu_{10}Te_4S_{13}$, the entire spectrum shifts towards higher energies with decreasing temperature as expected within a quasi-harmonic model in which the progressive contraction of the unit cell results in a hardening of the phonons energies. In $Cu_{12}Sb_2Te_2S_{13}$, the vibrational modes above ~ 6 meV behave similarly. Below 6 meV, however, the additional low-energy mode shows the opposite trend, *i.e.* a strong decrease in its characteristic energy upon cooling (Fig. 4c). This anomalous softening is suppressed below 50 K where the energy of the phonon locks in at ~ 2.5 meV. The significant loss in intensity of this peak upon heating is a direct consequence of the larger ADP of Cu2 (see Tables 1 and 2 in Electronic Supplementary Information). This ADP suppresses the signal of Cu2 in the INS experiments through the Debye-Waller factor,[35] thereby providing a strong experimental evidence for the dominating character of Cu2 dynamics in the low-energy excitations.

A comparison between the large softening undergone by this mode and available data on cage-like compounds is shown in Fig. 4d where the temperature dependence of its characteristic energy is plotted along with two theoretical curves calculated from the model proposed by Dahm and Ueda.[36] This model has been widely employed in highly anharmonic cage-like materials and offers the possibility to quantify the strength of the anharmonicity through a dimensionless parameter b. The predicted $w(T)$ curves calculated with b = 0.1 and 0.5 agree qualitatively with our experimental data indicating that b is close to 0.5. This

value is of comparable magnitude with that observed in the KOs_2O_6 pyrochlore ($b \sim 0.7$), a cage-like material known to be highly anharmonic.[37] Yet, a unique value of this parameter seems insufficient to describe the whole temperature range of our experimental data, which hints at a temperature-dependent potential energy.

IV. Discussion and conclusions

In this last section, we discuss the possible mechanisms that may play explain the significant loss of anharmonicity in $Cu_{10}Te_4S_{13}$ with respect to $Cu_{12}Sb_2Te_2S_{13}$. A first possibility arises from the unusual three-fold coordination of the Cu2 atoms, which frustrates the overlap between the *p*-states of S atoms and the *d*-states of Cu. The presence of vacancies (two per formula unit) could result in atomic relaxations of the Cu2 atoms, thereby removing the frustration.

The second possible effect is tied to the electrostatic field generated by the electronic densities around the two apical metalloids. Even though the Cu2 atoms do not form a chemical bonding with the metalloids, their out-of-plane displacements likely create electric dipoles, which interact with those induced by the electronic lone pairs present on the metalloids. Indeed, both cations (Te and Sb) feature a filled $5s^2$ electron pair. Yet, fundamental differences exist between the stereochemical activity of the lone pairs in the (Sb, Te) – S bonding. As reviewed by Wash *et al.*[38], the formation of stereochemically active lone pairs depends on the strength of the interaction between the cation *s*-states and the anion *p*-states, and hence, on their relative energies. This scenario is consistent with electronic band structure calculations that confirm the lower energy of the 5*s* atomic orbital of Te compared to Sb that weakens the 5*s* – 3*p* on-site hybridization in the Te – S bonding (see Figure 3 in

Electronic Supplementary Information). Even though their microscopic origin is different, dipolar electrostatic interactions have been proposed to play a decisive role in the transition from crystal-like to glass-like thermal conductivity in clathrates, another well-known family of cage-like thermoelectric materials with low thermal conductivity.[39] We note that this mechanism is corroborated by the recent study of Lai *et al.*[31] By combining high-resolution synchrotron XRD and density functional theory calculations, these authors have demonstrated that the lone-pair electrons of Sb result in local bonding asymmetry which leads to the out-of-plane anharmonic mode evidenced by our INS and Raman data.

Another ingredient that may play a role is a possible off-plane split position of the Cu2 atoms as suggested by Suekuni *et al.*[28] from the temperature dependence of the ADPs in the Ni-substituted tetrahedrites $Cu_{12-x}Ni_xSb_4S_{13}$. This proposition echoes that formulated by Pfitzner *et al.*[40] based on a detailed study of the evolution of the crystal structure of the $Cu_{12}Sb_4S_{13}$ tetrahedrite at high temperatures. The Cu2 atoms would then feel a double-well potential resulting in strong anharmonicity.[41,42]

All these effects might concomitantly contribute to the disappearance of the anharmonicity in $Cu_{10}Te_4S_{13}$, which governs the behaviour of the thermal transport in tetrahedrites. Further experimental and theoretical investigations are nevertheless necessary to determine the extent to which each of them contributes.

Acknowledgements

The authors would like to thank the Institut Laue Langevin and the Laboratoire Léon Brillouin for the support of this work and the grant of accessing the IN6, IN4 and 2T inelastic neutron scattering instruments.

References

1. T. Siegrist, P. Merkelbach and M. Wuttig, *Annu. Rev. Condens. Matter Phys.*, 2012, **3**, 215.
2. T. Matsunaga, N. Yamada, R. Kojima, S. Shamoto, M. Sato, H. Tanida, T. Uruga, S. Kohara, M. Takata, P. Zalden, G. Bruns, I. Sergueev, H. C. Wille, R. P. Heremann and M. Wuttig, *Adv. Funct. Mater.*, 2011, **21**, 2232.
3. *Thermoelectrics and its Energy Harvesting,* edited by D. M. Rowe (CRC Press, 2012).
4. G. J. Snyder and E. S. Toberer, *Nature Mater.*, 2010, **7**, 105.
5. H. J. Goldsmid in *Thermoelectric Refrigeration* (Temple Press Books, Ltd.: London, 1964).
6. D. Schmitt, N. Haldolaarachchige, Y. Xiong, D. P. Young, R. Jin and J. Y. Chan, *J. Am. Chem. Soc.*, 2013, **134**, 5965.
7. S. R. Brown, S. M. Kauzlarich, F. Gascoin and J. G. Snyder, *Chem. Mater.*, 2006, **18**, 1873.
8. S. K. Bux, A. Zevalkink, O. Janka, D. Uhl, S. Kauzlarich, J. G. Snyder and J.-P Fleurial, *J. Mater. Chem. A*, 2014, **2**, 215.
9. D. T. Morelli, V. Jovovic and J. P. Heremans, *Phys. Rev. Lett.*, 2008, **101**, 035901.
10. P. Gougeon, P. Gall, R. Al Rahal Al Orabi, B. Fontaine, R. Gautier, M. Potel, T. Zhou, B. Lenoir, M. Colin, C. Candolfi and A. Dauscher, *Chem. Mater.*, 2012, **24**, 2899.
11. M. Christensen, A. B. Abrahamsen, N. S. Christensen, F. Juranyi, N. H. Andersen, K. Lefmann, J. Andreasson, C. R. H. Bahl, B. B. Iversen, *Nature Mater.*, 2008, **7**, 811.

12. G. A. Slack and V. G. Tsoukala, *J. Appl. Phys.*, 1994, **76,** 1665; G. A. Slack in *CRC Handbook of Thermoelectrics* (ed. D. M. Rowe) 407–440 (CRC Press, Boca Raton, 1995).

13. H. Euchner, S. Pailhès, L. T. K. Nguyen, W. Assmus, F. Ritter, A. Haghighirad, Y. Grin, S. Paschen and M. de Boissieu, *Phys. Rev. B*, 2012, **86**, 224303.

14. S. Pailhès, H. Euchner, V. M. Giordano, R. Debord, A. Assy, S. Gomès, A. Bosak, D. Machon, S. Paschen and M. de Boissieu, *Phys. Rev. Lett.*, 2014, **113**, 025506.

15. O. Delaire, J. Ma, K. Marty, A. F. May, M. A. McGuire, M.-H. Diu, D. J. Singh, A. Podlesnyak, G. Ehlers, M. D. Lumsden and B. C. Sales, *Nature Mater.*, 2011, **10**, 614.

16. M. D. Nielsen, V. Ozolins and J. P. Heremans, *Energy Environ. Sci.*, 2013, **6**, 570.

17. E. J. Skoug, D. T. Morelli, *Phys. Rev. Lett.*, 2011, **107**, 235901.

18. S. Lee, K. Esfarjani, T. Luo, J. Zhou, Z. Tian, G. Chen, *Nature Comm.*, 2014, **5**, 3525.

19. J. Ma, O. Delaire, A. F. May, C. E. Carlton, M. A. McGuire, L. H. VanBebber, D. L. Abernathy, G. Ehlers, T. Hong, A. Huq, W. Tian, V. M. Keppens, Y. Shao-Horn and B. C. Sales, *Nature Nanotech.*, 2013, **8**, 445.

20. K. F. Hsu, S. Loo, F. Guo, W. Chen, J. S. Dyck, C. Uher, T. Hogan, E. K. Polychroniadis, M. G. Kanatzidis, *Science*, 2004, **303**, 818.

21. P. G. Klemens in *Thermal Conductivity and Lattice Vibrational Modes* (Solid State Physics, Academic, New York, 1958).

22. D. T. Morelli and G. A. Slack in *High Thermal Conductivity Materials* (eds. S. Shinde, J. Goela) Ch. 2, 37 – 64 Springer: New York, NY, USA (2005).

23. M. C. Roufosse and P. G. Klemens, *Phys. Rev. B*, 1973, **7**, 5379.

24. J. W. Miller, J. R. Craig, *Am. Mineral.*, 1983, **68**, 227.

25. X. Lu, D. T. Morelli, Y. Xia, F. Zhou, V. Ozolins, H. Chi, X. Zhou and C. Uher, *Adv. Energy Mater.*, 2013, **3**, 342.

26. X. Lu and D. T. Morelli, *Phys. Chem. Chem. Phys.*, 2013, **15**, 5762.

27. K. Suekuni, K. Tsuruta, T. Ariga and M. Koyano, *Appl. Phys. Exp.*, 2012, **5**, 051201.

28. K. Suekuni, K. Tsuruta, M. Kunii, H. Nishiate, E. Nishibori, S. Maki, M. Ohta, A. Yamamoto, M. Koyano, *J. Appl. Phys.*, 2013, **113**, 043712.

29. J. Heo, G. Laurita, S. Muir, M. A. Subramanian and D. A. Keszler, *Chem. Mater.*, 2014, **26**, 2047.

30. E. Lara-Curzio, A. F. May, O. Delaire, M. A. McGuire, X. Lu, C.-Y. Liu, E. D. Case and D. T. Morelli, *J. Appl. Phys.*, 2014, **115**, 193515.

31. W. Lai, Y. Wang, D. T. Morelli and X. Lu, *Adv. Funct. Mater.* DOI: 10.1002/adfm.201500766 (2015).

32. X. Fan, E. D. Case, X. Lu and D. T. Morelli, *J. Mater. Sci.*, 2013, **48**, 7540.

33. C. H. Lee, I. Hase, H. Sugawara, H. Yoshizawa, H. Sato, *J. Phys. Soc. Jpn.*, 2006, **75**, 123602.

34. T. Tadano, Y. Gohda, S. Tsuneyuki, *Phys. Rev. Lett.*, 2015, **114**, 095501.

35. M. M. Koza, A. Leithe-Jasper, H. Rosner, W. Schnelle, H. Mutka, M. R. Johnson, Yu. Grin, *Phys. Rev. B*, 2014, **89**, 014302.

36. T. Dahm and K. Ueda, *Phys. Rev. Lett.*, 2007, **99**, 187003.

37. H. Mutka, M. M. Koza, M. R. Johnson, Z. Hiroi, J.-I. Yamaura, Y. Nagao, *Phys. Rev. B*, 2008, **78**, 104307.

38. A. Wash, D. J. Payne, R. G. Egdell, G. W. Watson, *Chem. Soc. Rev.*, 2011, **40**, 4455.

39. T. Takabatake, K. Suekuni, *Rev. Mod. Phys.*, 2014, **86**, 669.

40. A. Pfitzner, M. Evain and V. Petricek, *Acta Cryst.*, 1997, **B53**, 337.

41. D. J. Safarik, T. Klimczuk, A. Llobet, D. D. Byler, J. C. Lashley, J. R. O'Brien, N. R. Dilley, *Phys. Rev. B*, 2012, **85**, 014103.

42. D. J. Safarik, A. Llobet, J. C. Lashley, *Phys. Rev. B*, 2012, **85**, 174105.

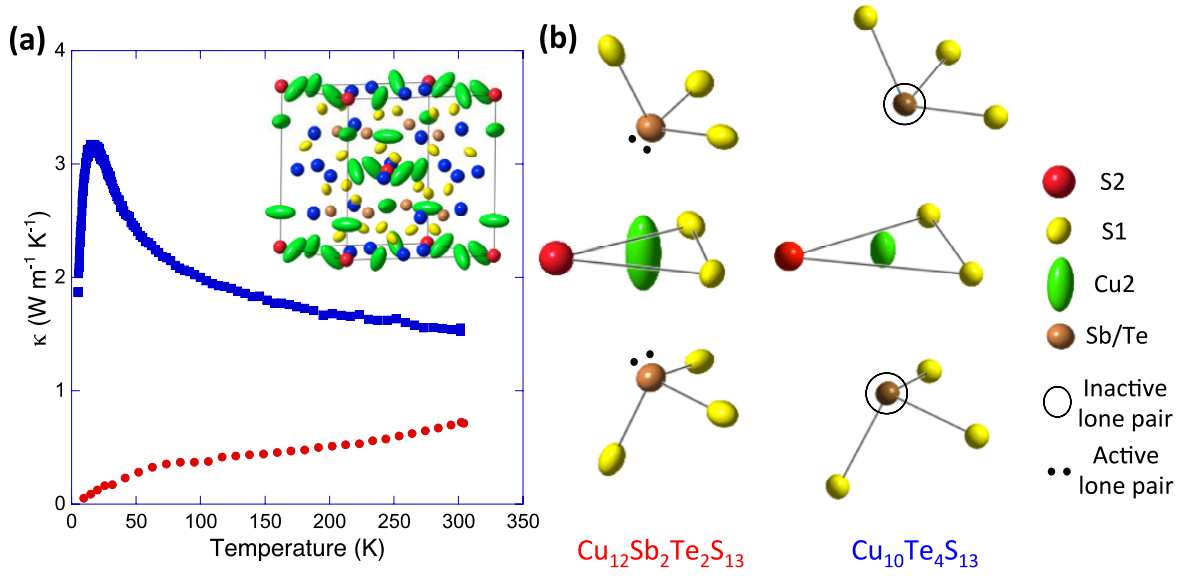

Figure 1. Transition from crystalline-like to glass-like thermal conductivity. **(a)** Temperature dependence of the lattice thermal conductivity k_L of $Cu_{12}Sb_2Te_2S_{13}$ (●) and $Cu_{10}Te_4S_{13}$ (■). (Inset) Perspective view of the cubic crystal structure of tetrahedrites drawn in an ellipsoid representation that highlights the anisotropic thermal displacement parameter of the Cu2 atoms. **(b)** Atomic environment of the Cu2 atoms in $Cu_{12}Sb_2Te_2S_{13}$ and $Cu_{10}Te_4S_{13}$. The thermal ellipsoids are drawn at the 50% probability level. Note that the Sb or Te atoms and the Cu2 atoms do not form a chemical bonding. The $5s^2$ electron lone pairs revolving around the Sb and Te atoms are also sketched. Because the Te lone pair is inert, the original spherical symmetry of the $5s^2$ electrons is retained in the Te – S bonds. Unlike the Te lone pairs, the Sb lone pairs are active: the Sb($5s$) – S($3p$) hybridization breaks the spherical symmetry.

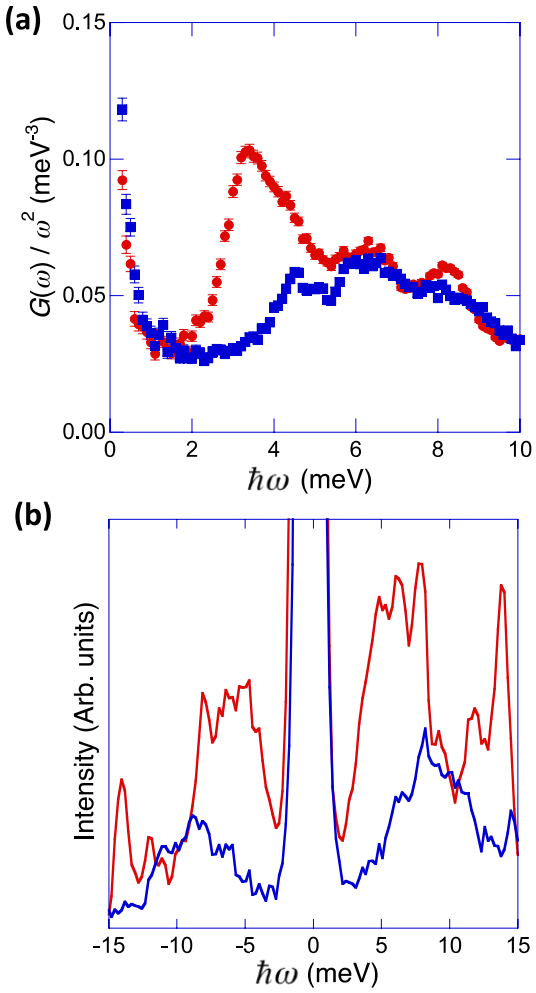

Figure 2. Excess vibrational modes in $Cu_{12}Sb_2Te_2S_{13}$. **(a)** Generalized density of states $G(w)$ of $Cu_{12}Sb_2Te_2S_{13}$ (red circles) and $Cu_{10}Te_4S_{13}$ (blue squares) measured at 300 K shown in a Debye presentation $G(w)/w^2$. **(b)** Raman spectra of $Cu_{12}Sb_2Te_2S_{13}$ (red) and $Cu_{10}Te_4S_{13}$ (blue) measured at the Stokes and anti-Stokes line.

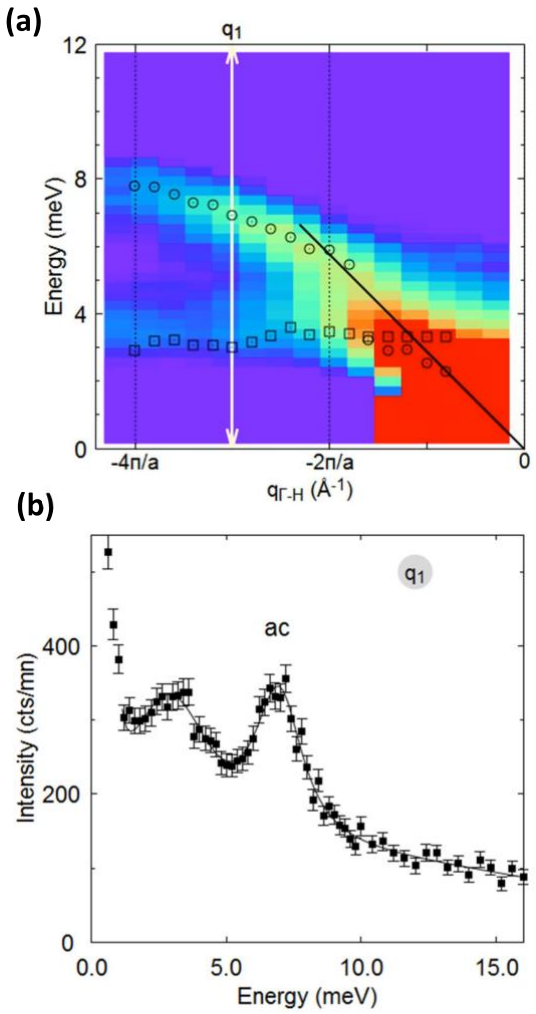

Figure 3. Mapping of the $TA^{(100)}_{(011)}$ phonons measured in a natural, single-crystalline tetrahedrite specimen. **(a)** Experimental neutron intensities (background subtracted) represented as a false color image as a function of the wave vector and energy (sp2T@LLB). Black open circles and squares represent the fitted experimental positions for the TA and optic phonons, respectively. **(b)** Raw data of constant energy scan performed at a constant wave vector $|q_1| = 0.91$ Å^{-1}. The measured scattering profiles were fitted using damped harmonic oscillators for acoustic phonons (labeled "ac") and Gaussian functions for the low-lying optical excitations.

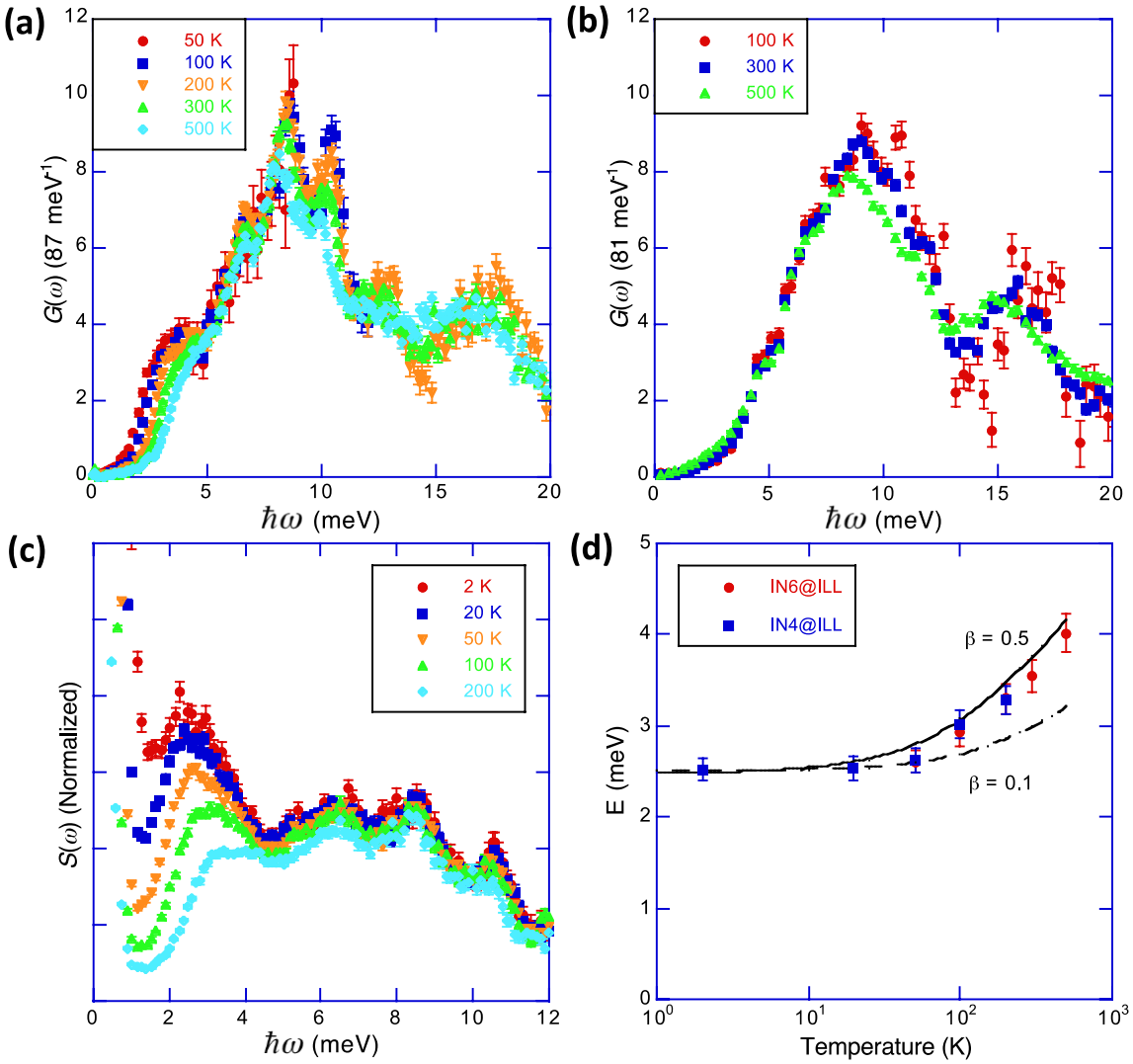

Figure 4. Inelastic neutron scattering data of $Cu_{10}Te_4S_{13}$ and $Cu_{12}Sb_2Te_2S_{13}$. **(a)** Temperature dependence of $G(w)$ of $Cu_{12}Sb_2Te_2S_{13}$ between 50 and 500 K measured on IN6@ILL. **(b)** Evolution of $G(w)$ measured on IN6@ILL as a function of temperature for $Cu_{10}Te_4S_{13}$. In both panels, the data were normalized to 87 and 81 phonon modes, respectively. **(c)** Dynamic structure factor measured down to 2 K at the Stokes line (IN4@ILL) for $Cu_{12}Sb_2Te_2S_{13}$. The temperatures color-coded are indicated in the legend of the figures. **(d)** Temperature dependence of the maxima of the low-energy peak observed in the $Cu_{12}Sb_2Te_2S_{13}$ compound on a logarithmic scale. The black dotted and solid lines stand for the theoretical temperature dependence derived from the theory of Dahm and Ueda (Ref. 36) with anharmonicity

parameters of b = 0.1 and 0.5, respectively. The data of IN6 has been scaled up to match the IN4 data at intermediate temperatures in order to account for the different energy resolution and phase space covered by the two instruments.